Analysis of the Stress between Implant Prostheses with Different Moduli and Surrounding Bones

Ye Zhu (18604499241@163.com)
Dalian Jiaotong University

Yixin Shao
Dalian Jiaotong University

Tianmin Guan
Dalian Jiaotong University

Bing Lin
Dalian Stomatological Hospital

Chongyang Guo
Dalian Jiaotong University

Ting Pan
Qingdao University of Science and Technology

Research Article

Keywords: Stress shielding, Bone model, Biomechanical simulation, Gradient assignment

Posted Date: March 2nd, 2022

DOI: https://doi.org/10.21203/rs.3.rs-1358844/v1

Abstract

Stress shielding effect is the main factor affecting the effect of implant prosthesis repairing, and its main reason is that the elastic modulus of implanted prosthesis is greater than that of the surrounding bone tissues. In order to solve this problem, the influence of elastic modulus difference on the stress shielding was analyzed. A bone tissue model of the research object was obtained by CT scanning and optimized, then the gradient assignment was carried out to establish a more reliable bone mechanics model, and the model was combined with the implanted prosthesis for finite element simulation. Firstly, the finite element simulation of Beagle dog bone models, human bone model and the corresponding implant prostheses was carried out to simulate the stress and displacement distribution of prostheses with different elastic moduli after the implant prosthesis repairing. Secondly, the reasons for the stress shielding phenomenon caused by small elastic modulus differences were analyzed, the bone model and implant prosthesis model were constructed, and the method for the assignment of material properties was established. Finally, the feasibility of the model and the method for the assignment of material properties were verified, and the effects of the relationship between the elastic modulus of implant prostheses and that of bones on the formation of stress shielding were analyzed quantitatively in a way of randomly selecting stress points.

1 Introduction

Titanium alloy is widely used to make an implant prosthesis because of its low-density and high-strength mechanical properties, good biocompatibility and corrosion resistance. The use of titanium alloy implant prosthesis has become an important medical means to treat bone defects, especially Ti-6Al-4V that has been recognized as the most suitable titanium alloy material for repairing bone defects due to its tensile strength, corrosion resistance and biocompatibility higher than those of other titanium alloys at present, and its elastic modulus can be significantly reduced by making it into a porous structure to make its elastic modulus closer to that of human bones to help to repairing human bone defects [1-3]. At present, a variety of porous titanium alloy orthopedic implant prostheses processed by 3-Dimetional printing have been approved for listing, such as knee implant prosthesis, ankle implant prosthesis, hip implant prosthesis, maxillofacial implant prosthesis and spine implant prosthesis, with a satisfied clinical application effect [4, 5]. It is well known that when the elastic modulus of an implanted prosthesis is higher than that of a human bone, the stress will more concentrated on the implanted prosthesis, resulting in less stress on the human bone. In this case, the absorption of bone tissue will take place to form a stress shielding phenomenon due to the small stress on the human bone at this time according to Wolff's law and adaptive elasticity theory, and on the contrary, if the elastic modulus of the implanted prosthesis is lower than that of the human bone, the stress will more concentrated on the human bone, and the human bone is prone to damage due to the excessive stress, so only when the elastic modulus of the implanted prosthesis is consistent with the human bone can it be more conducive to bone ingrowth [6-9]. Due to these reasons, a lot of studies in this field have been conducted by scholars. For example, in 2016, Li et al. [10] proved that a stent with a porosity of 300 ~ 400 μM was conducive to bone growth; In 2013,

Melchels et al. [11] confirmed through mechanical experiments that when the porosity of the implanted prosthesis was 61.5%, its elastic modulus was 3.1 GPa, close to that of human cancellous bone; The study of Chlebus et al. [12] showed that porous structure could significantly reduce the elastic modulus of titanium alloy, and the modulus could be adjusted according to porosity; Parthasarathy et al. [13] realized the regulation of mechanical properties of porous titanium alloy to a certain extent. Many scholars have made great achievements in reducing the elastic modulus of titanium alloy to adapt it to human bone, and they have not made the elastic modulus of implanted prosthesis completely consistent with that of repaired bone, although many mathematicians have adjusted the elastic modulus of implanted prosthesis to the elastic modulus of human cortical bone. To our best knowledge, there are few reports on whether the implanted prosthesis meeting this range of elastic modulus can effectively eliminate the stress shielding effect, and few scholars have established reliable mechanical models of implanted prosthesis and bone so far.

This study mainly included □ the establishment and optimization of an experimental bone tissue model by CT scanning, □ the gradient assignment of material properties for the optimized model and the establishment of a mechanical model consistent with the mechanical properties of the experimental bone, and □ the analysis on the mechanical model after adding the implanted prosthesis by finite element method, and the observation on the mechanical differences of prostheses with different elastic moduli under stress, which was expected to provide a theoretical basis for further optimizing the implanted prosthesis and completely eliminating the stress shielding phenomenon.

2 Objects And Methods

2.1 Research objects

One-year-old healthy beagle dogs were selected for the experiment, and the bone models from two volunteers were obtained for the study, in which a male volunteer was 27 years old and another female volunteer was 57 years old.

2.2 Animal experimental bone model

In order to obtain a complete and real bone model of the animal research objects, the bone model of experimental dogs was identified by CT scanning, and the dogs were anesthetized by the intravenous injection of dexmedetomidine and Zoletil 20. The bones of dogs were scanned with a Scintcare CT16 X-ray computed tomography equipment (Zhejiang Mingfeng Medical System Co., Ltd., China), in which the scanning layer thickness was 1 mm. The scanned image file was saved in DICOM3.0 format, and the dogs were awakened by the intravenous injection of atimidazole hydrochloride.

Mimics19.0 software was used to process the CT images obtained by scanning since the software could quickly segment the CT images based on the threshold. According to the experience of other scholars [14-

16] and combined with the built-in parameter analysis by Mimics software, the gray value range was set at 156-2198Hu for extraction, and the extracted model is shown in Fig. 1A. However, it could be found that the model was rough and there were many redundant fragments, indicating that the model could not be used for the subsequent finite element analysis. Therefore, Geomagic wrap2017 software was used for the processing and optimization to delete the irrelevant fragments and bottom plates. As shown in Fig. 1B, the image of processed model was relatively clear, and the bones more suitable for follow-up research could be selected for further processing. After screening, the leg bones of the experimental dogs were selected as the main research objects and numbered (Fig. 2). Geomagic software was used to refine each bone, respectively. Taking the left front thigh bone (LF1) as an example, as shown in Fig. 3A and B, the original rough burrs and holes were removed in the processed model, which could not only maintain the characteristics of the original bone, but also provide a model with high accuracy for the establishment and analysis of subsequent finite element models.

2.3 Construction of implant prosthesis models

In order to better compare the effects of different elastic moduli on the stress distribution of implanted prostheses and human bone, Geomagic software was used to directly intercept parts of models on the main studied bones as the implanted prosthesis model, and this method could make the implanted prosthesis more consistent with the human bone model and eliminate the influence of irrelevant factors such as the loose combination of models to better ensure the reliability of data. Taking LF1 as an example, as shown in Fig. 4, placing two implant prostheses on the same bone, namely the corresponding cortical model A1 and cancellous bone model A2 in one group, and the corresponding cortical bone model B1 and cancellous bone model B2, could better analyze the mechanical properties of different positions. Furthermore, in subsequent animal experiments, the two implant prostheses could be used for comparing the mechanical properties of implant prostheses while ensuring the blood supply. Therefore, two implant prostheses were set on the same bone in this study, as shown in Fig. 4C.

2.4 Model grid division

In order to better carry out the follow-up mechanical experiments, the NURBS surface fitting was conducted for the optimized main research bone and implant prosthesis models. The grid division was performed by using by using the generated entity application software HyperMesh 2017, and the quality of grids was checked by elements. The inspection standards are as follows: warpage < 15 °; aspect ratio ≤ 5°; min angle tria ≥ 30°; max angle tria ≤ 120°; jacobian > 0.6; taper 0.6.

2.5 Assignment of model material properties

For research objects, the leg bones jointly bear all the weight of the body, and the bones are mainly composed of cortical bone and cancellous bone; in addition, the bone material properties of this part are

anisotropic, so scholars have also used a variety of methods for the assignment of material properties [14–17]. It has been shown that there is a linear relationship between the bone elastic modulus and the bone ash value [18]. In this paper, the gradient assignment was adopted by using Mimics software combined with the calculation of the bone ash value. The assignment methods are as follows.

Poisson's ratio assignment:

$$\nu = 0.3 \tag{1}$$

Density assignment when the gray value is 101 and less than 101:

$$\rho = 50 + 0 \bullet Hu \tag{2}$$

Elastic modulus assignment:

$$E = 0.004 \cdot \rho^{2.01} \tag{3}$$

Density assignment of femur when the gray value is 102 and more than 102:

$$\rho = 131 + 1.067 \cdot Hu \tag{4}$$

Elastic modulus of femuris:

$$E = 0.01 \cdot \rho^{1.86} \tag{5}$$

Density assignment of tibia and fibula:

$$\rho = 114 + 0.916 \cdot Hu \tag{6}$$

Elastic modulus of femur:

$$E = 0.51 \cdot \rho^{1.37} \tag{7}$$

Where ρ is the apparent density in the image obtained by CT scanning (g/cm^3); Hu is the gray value of bones; E is the elastic modulus of the main research bones (MPa). The gray values of the main research

bones in CT scanning data could be obtained by using the material assignment function in Mimics software, the mechanical properties of the main research bones could be understood based on the calculation using formula (1-6), and the assignment of ten gradient elastic moduli to the bone finite element model could be completed according to the gray value. Taking the assignment results of LF1 as an example, the effect after the assignment of the bone model is shown in Fig. 5A, and the material properties corresponding to the ten materials are shown in Fig. 5B.

Based on the data obtained from CT model, in ABAQUS finite element simulation software, the models of implanted prostheses were distinguished according to cortical bone and cancellous bone, and the material properties were assigned. An experimental group and a control group were set up, and the mechanical properties in the experimental group were consistent with the average values of mechanical properties of nearby multi-point bones. The control group was divided into control group A and control group B, and the elastic modulus in control group A was greater than that of nearby bones, and the elastic modulus in control group B was less than that of nearby bones. The specific values of cortical bone and cancellous bone implant prostheses of main research bones are shown in Table 1, and the data units all are MPa. Among them, the elastic modulus in control group A was greater than that of nearby bones, and the elastic modulus of cortical bone in control group B was 5000 MPa larger than that of nearby bones. Because the elastic modulus of cancellous bone itself was small, the difference in the elastic modulus between control group A or control group B and the experimental group was positive 1000 MPa and negative 1000 MPa, respectively.

Table 1

Assignment results of material properties of bones in the experimental and control groups (MPa)

Number of bones	Average modulus	Experimental group	Control group A	Control group B
LF1 (cortical)	12596	12596	17596	7596
LF1 (cancellous)	3944	3944	4944	2944
LF2 (cortical)	12955	12955	17955	7955
LF2 (cancellous)	4206	4206	5206	3206
LF3 (cortical)	13129	13129	18129	8129
LF3 (cancellous)	4799	4799	5799	3799
LB1 (cortical)	14153.4	14153.4	19153.4	9153.4
LB1 (cancellous)	2790	2790	3790	1790
LB2 (cortical)	15830.8	15830.8	20830.8	10830.8
LB2 (cancellous)	5634	5634	6634	4634
RF1 (cortical)	12596	12596	17596	7596
RF1 (cancellous)	3944	3944	4944	2944
RF2 (cortical)	12955	12955	17955	7955
RF2 (cancellous)	4206	4206	5206	3206
RF3 (cortical)	13129	13129	18129	8129
RF3 (cancellous)	4799	4799	5799	3799
RB1 (cortical)	14153.4	14153.4	19153.4	9153.4
RB1 (cancellous)	2790	2790	3790	1790
RB2 (cortical)	15830.8	15830.8	20830.8	10830.8
RB2 (cancellous)	5634	5634	6634	4634

2.6 Setting of external load

Boundary conditions: Restraining the degrees of freedom in six directions of the lower end face of each main research bone; Applied load: The upper surface of each main research bone was coupled to one point, and a vertical downward axial load was applied. The applied axial load was 70 N since the weight of experimental dogs was 10 kg, and considering that the two feet would be always on the ground during the movement, with a certain impact force. The displacement change and stress distribution in each experimental group and the control group were compared and analyzed.

2.7 Obtaining the bone model of subjects

Similar to the method of obtaining the animal experimental bone model, the bone model of volunteer subjects was obtained by CT scanning. The bones of a male volunteer and a female volunteer were scanned by a ScintCare CT16 X-ray computed tomography equipment, in which the scanning layer thickness was 1 mm, and the scanned images were saved as DICOM3.0 format and processed with Mimics19 0 software to extract the models, as shown in Fig. 6A. The results showed that the extracted models were rough and it was difficult for them to be used for the follow-up studies. Then, the subject thigh bones were selected for processing, and the redundant fault surfaces were deleted and the missing fault surfaces were repaired by using a Geomagic wrap2017 software. As shown in Fig. 6B, the repaired models were more flat and smooth on the premise of retaining the shape and characteristics of the original models, which were considered to be able to provide high-quality models for the subsequent finite element analysis.

2.8 Finite element simulation of implant prosthesis stress of human bone model

In the similar way to that used for the animal bone model, the implant prosthesis model was established, the model grid division was carried out and the model material properties were assigned. Geomagic software was used to intercept parts of the model from the main research bones as the implant prosthesis model for the comparison among the three groups. The specific values of cortical bone and implant prosthesis are shown in Table 2. Bones in the experimental group and the control group were loaded, respectively, in which the weight of the male volunteer was 90 kg and that of the female volunteer was 60 kg. According to the adult human body inertia parameters issued by Standardization Administration of China in 2004 (Fig. 7) [19], an additional load was applied as shown in Table 2 because people were considered to have more time to land on one foot during walking.

Table 2

Assignment results of human bones in the experimental and control groups

Bone models	Bone modulus	Experimental group	Control group (1)	Control group (2)	Load (N)
Male	18479	18479	28479	8479	711
Female	18039	18039	28039	8039	472

3 Results

3.1 Comparative analysis of stress distribution and displacement changes of implanted prosthesis in Beagle dog bone model

In this paper, an experimental dog bone model with a high accuracy was established and assigned in more detail, and the stress change of the leg during daily walking of the experimental dogs was simulated. The influence on the implant prosthesis and bone connection was analyzed by applying an axial force load. Due to the small stress in the horizontal direction during walking, this paper focused on the study on the changes of displacement and stress of bone under a vertical load. As shown in Table 3, taking the displacement change and stress distribution of bone LF2 as an example, the implanted prosthesis with different elastic moduli could be affected by the displacement change between the implanted prosthesis model and the bone model after being loaded. In order to more effectively compare the influence, a chart column was drawn in Fig. 8. As shown in Fig. 8, the displacement of the whole bone model decreased after the elastic modulus of the implanted prosthesis increased, and the displacement of the whole bone model increased after the elastic modulus of the implanted prosthesis decreased. However, it should be considered that the implanted prosthesis with different elastic moduli might have a little effect on the displacement between the prosthesis and bone after operation, and the screw-assisted fixation was considered to often be used to ensure the stability of the connection between the prosthesis and bone during the operation of repairing bone defects, suggesting that the possibility of prosthesis falling off due to the poor displacement caused by the elastic modulus of implanted prosthesis could be ignored temporarily. As shown in Table 3, although it was impossible to determine the location of the maximum stress by observing the color, it could be seen that the implanted prosthesis with different elastic moduli might have a certain impact on the stress distribution after loading, in which the stress concentrated on the implanted prosthesis model increased when the elastic modulus of the implanted prosthesis was greater than that of the bone and the stress concentrating on the implant prosthesis model decreased when the elastic modulus of implant prosthesis was less than that of bone, but the stress near the implant prosthesis model increased, and moreover, the impact was much more obvious than that of the elastic modulus of the implanted prosthesis on the displacement change. As shown in Table 3, although the elastic modulus of the implanted prosthesis was only slightly greater than that of the bone and still within the range of the elastic modulus of the bone, the stress still obviously concentrated on the prosthesis, resulting in a stress shielding and then a poor postoperative recovery of the patients, even the falling off of prosthesis due to the osteoporosis around the implanted prosthesis. On the contrary, even if the elastic modulus of the implanted prosthesis was only slightly greater than that of the bone and still within the range of bone elastic modulus, the stress would still concentrated on the bone around the implanted prosthesis, leading to a secondary damage to the patient's bone.

The finite element simulation results could not only illustrate the influence of the elastic modulus difference between the implanted prosthesis and the bone on the overall displacement and stress distribution, but also show the establishment of a more reliable Beagle dog bone model and the implanted prosthesis model, and establish a method for the assignment of material properties. The

material properties assigned by this method should be more detailed and close to the mechanical properties of the bone model.

Table 3

Changes of displacement and stress distribution of bone LF2

Simulation	Experimental group	Control group A	Control group B
Displacement change	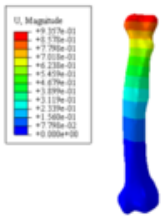	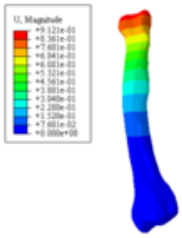	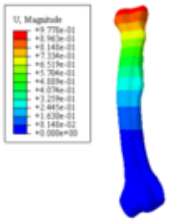
Stress distribution	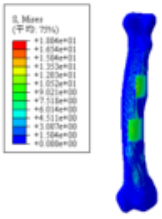	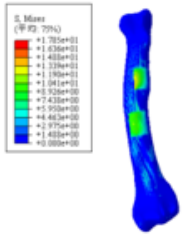	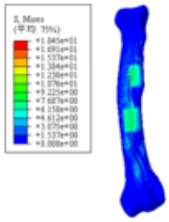

Maximum displacement（mm）

3.2 Comparative analysis of stress distribution of implanted prosthesis in human bone model

In the similar way to obtaining the Beagle dog bone model, a more refined volunteer bone model was obtained for its optimization, grid division and material property assignment, and a small part of the model was intercepted for the mechanical simulation of simulated implant prosthesis to assign implant prostheses with different elastic moduli, simulate the stress process of human bone and implant prosthesis during upright walking (Table 4). Because the finite element simulation of Beagle dog bone had shown that under the premise of bone constraints and the close contact between the implant prosthesis and bone, the displacement change would be not obvious, the finite element simulation of human bone simulated implant prosthesis focused on the analysis of stress distribution. It could be seen in the stress distribution of the previous three groups of finite element simulation (Table 3) that the stress on the implanted prosthesis was relatively concentrated, but the specific stress values could not be clearly compared. Therefore, the points on the implanted prosthesis and the corresponding points on the surrounding bones were selected to obtain the stress values. The points on the upper, lower, left and right directions of the implanted prosthesis and those on the human bones connected to it were selected, 2 points in each direction, and the specific points are shown in Fig. 9A. As shown in Fig. 9, a represents the

8 points selected on the implanted prosthesis and b represents the corresponding 8 points selected on the human bone. Finite element simulations of male and female bone models as well as implanted prosthesis were carried out with ABAQUS software, and The charts (Fig. 9) of experimental results from these 16 points were made. Fig. 9A shows the bone stress distribution of male volunteers and Fig. 9B shows the bone stress distribution of female volunteers, in which A0a and A0b represent the stress distribution of implant prosthesis and male human bone in the experimental group, A1a and A1b represent the stress distribution of implant prosthesis and male human bone in the control group (1), and A2a and A2b represent the stress distribution of implant prosthesis and male human bone in the control group (2). The naming method in Fig. 9B is similar to that in Fig. 9A, and stress points 1-8 in it represent the corresponding stress points in Fig. 9(A), respectively. Stress points 1-8 could be clearly found, and when the elastic modulus of the implanted prosthesis was consistent with that of the human bone, A0a and Aa0b, B0a and B0b could be seen in Fig. 9 although the stress was not completely consistent with that at the corresponding points, indicating that when the elastic modulus of the implanted prosthesis is consistent with the human bone, the stress distribution may be more average and there will be less stress concentration; When the elastic modulus of the implanted prosthesis was inconsistent with that of the human bone, the stress distribution would be uneven. It can be understood from A1a and A1b, B1a and B1b in Fig. 9 that when the elastic modulus of the implanted prosthesis is greater than that of the human bone, the stress will concentrate on the implanted prosthesis and the stress shielding will occur. A2a and A2bB, B2a and B2b in Fig. 9 indicate that when the elastic modulus of the implanted prosthesis is less than that of the human bone, the stress will concentrate on the human bone, easily leading to the secondary fracture, and even if the elastic modulus of the implanted prosthesis meets the range of the elastic modulus of the human bone, the stress concentration is still very obvious, and even the stress difference is more than 100%, which is very unsatisfactory for the postoperative rehabilitation of the implanted prosthesis to repair the bone injury. Therefore, the above situation can be prevented only if the elastic modulus of the implanted prosthesis is consistent with that of the bone in the implanted area, and in addition, the simulation results are also consistent with those of the stress shielding phenomenon in the process of repairing bone injury with implant prosthesis and the secondary fracture phenomenon when the elastic modulus of implant prosthesis is less than that of surrounding bone, demonstrating that the bone and implant prosthesis model and the material property assignment method established in the simulation process should be feasible.

Table 4

Stress distribution of human bones

No. of bones	Experimental group	Control group A	Control group B
Male	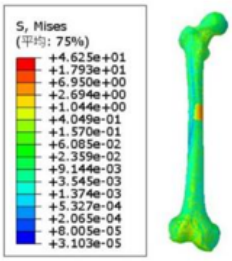	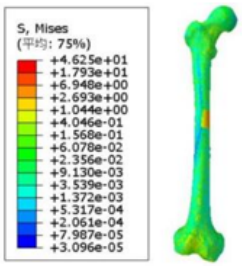	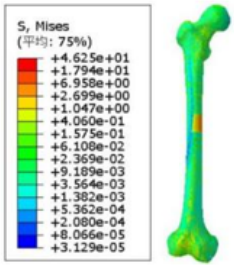
Female	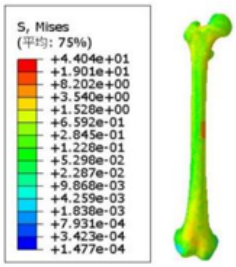	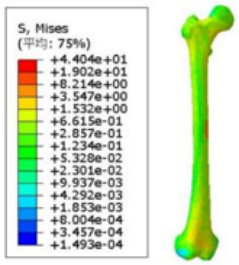	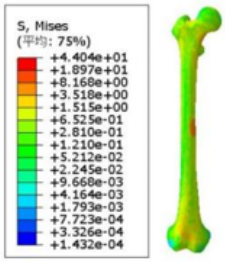

4 Discussion

Because the mechanical properties of the implanted prosthesis can directly affect the rehabilitation of patients with repairing bone defect with the implanted prosthesis, among which the elastic modulus of the implanted prosthesis is more important, the stress concentration and stress shielding may occur, even leading to the damage or falling-off of the implanted prosthesis and the failure of operation if the elastic modulus does not coincide with the elastic modulus of the bone near the implanted prosthesis, so that it is particularly important to accurately determine the elastic modulus of an implanted prosthesis and human bone [20]. In addition, bone model is of great significance for the orthopaedic research and clinical treatment of bone diseases, and the repair of bone defects with implanted prosthesis. At present, some scholars also focus on obtaining a human bone model in a reverse modeling way by CT scanning [21, 22]. However, the obtained model is often only the contour model of bones without the assignment of material properties, and the established bone model cannot be used for virtual simulation. Some scholars also focus on the material property assignment of bone model [14], but the established bone model has not been carefully optimized and there are some impurities on its surface, affecting the subsequent finite element simulation, and moreover, the specific differences of bones in different parts are not considered in the assignment of material properties to use the self-contained formula in Mimics software for the assignment of material properties, which has been considered relatively one-sided. Based on the bone model obtained by CT scanning, in this study, Geomagic software was used to optimize the model, parts of the bone were intercepted as the implant prosthesis model, and at the same time, the influence of bone complexity was considered to assign the gradient value to the bone and establish an implant prosthesis bone mechanics model. The changes of displacement and stress between the implanted prosthesis and

bone during the walking of the implant recipients were simulated, the solution was explored based on the causes of stress shielding, and the correctness of the theoretical model was verified, which was expected to provide a theoretical basis for the design of the mechanical property and structure of an implanted prosthesis in the process of repairing bone defects.

The method proposed in this paper was to obtain the bone model by CT scanning and Geomagic software was used to complete the optimization of the model. As shown in Fig. 3 and Fig. 6, although the interference of impurities on the model on the model quality and subsequent mechanical simulation could be eliminated, the small features on the original bone model could be inevitably deleted, so whether this method may affect the mechanical properties of the bone still needs to be further studied in the follow-up study. The proposed model was used for the grid division according to the ash value, and 10 materials were divided for the gradient assignment (Fig. 5). Although the model was very close to the actual situation of the bone model, there were still some errors in the simulation by gradient assignment undeniably due to the very complex properties of the bone as a special biomaterial and the smooth transition of its internal material properties, and the additional impact force in the process of human walking was not considered although the mass distribution of various parts of the human body was considered in the finite element simulation loading (Table 2), which should be further studied in the follow-up research.

In the mechanical simulation of human bone model after prosthesis implantation, the stress distribution between the implanted prostheses with different elastic moduli and the surrounding bones could be compared more accurately by comparing the stress between the implanted prosthesis and the bone model (Fig. 9), and this method could not only more accurately and quantitatively analyze the impact of implants with different elastic modulus on human bones, but also effectively verify the reliability of the established bone model. This method is rarely found in the research of other scholars.

In this paper, the experimental dog (Beagle Dog) and human bone were used for the finite element simulation, in which the effects of implanted prostheses with different elastic moduli on the displacement and stress distribution after the implant of prostheses were analyzed, and the feasibility of the established bone model in this paper was proved. This method is rarely found in the research of other scholars.

5 Conclusion

In this paper, in a way of establishing bone models of experimental dogs and human bodies and the mechanical finite element simulation of implanted prostheses, an effective scheme to eliminate stress shielding was explored, and the stress distribution of implanted prostheses and the surrounding bones after the bone defect repairing with implanted prostheses were simulated, verifying the reliability of the model, exploring the problems that should be paid attention to in the development of implanted prostheses, and proposing some solutions for them.

To sum up, ① A reliable and high-precision bone model that could be used for mechanical testing was established, and optimized; ② The gradient assignment of material properties of the optimized bone model was carried out by a more scientific gradient assignment method to make the assigned bone model closer to the real bone characteristics in mechanics; ③ The simulated mechanical experiments of dogs and subjects' bones with implant prostheses demonstrated that the implant of prostheses with different elastic moduli should have a little effect on the overall displacement of bone; ④ By randomly selecting the corresponding points on the implanted prostheses and surrounding bones, the influence of implanted prostheses with different elastic moduli on the stress distribution after the bone implant was quantified for the quantitative analysis on the effect of the relationship between the elastic modulus of prostheses and that of bones on the formation of stress shielding.

In this study, a reliable bone mechanics model was constructed, the influence of elastic modulus of implanted prosthesis on the displacement and stress distribution of bone was analyzed, and a solution to eliminate the stress shielding was established, which may provide a new idea for the treatment of repairing bone defects with an implant prosthesis.

Abbreviations

CT: Computed tomography;

Declarations

Acknowledgement

We gratefully acknowledge the support from the Liaoning Natural Science Foundation joint Fund project (2021-YGJC-10).

Authors' contributions

Shao yixin contributed to the acquisition, analysis and interpretation of data, and drafting the manuscript. Zhu Ye developed the study design. Pan Ting and Guo Chongyang participated in the acquisition and analysis of data. Lin Bing contributed to the surgery and the treatment of tested animals. Guan Tianmin contributed to research design, interpretation of data, drafting and revising the manuscript, and approval of the final submitted article. All authors have read and approved the final submitted manuscript.

Funding

This work was supported by the Liaoning Natural Science Foundation joint Fund project (2021-YGJC-10).

Availability of data and materials

The datasets used and/or analyzed during the current study are available from the corresponding author on reasonable request.

Ethics approval and consent to participate

All animal experiments comply with the ARRIVE guidelines and followed the U.K. Animals (Scientific Procedures) Act, 1986 and associated guidelines, EU Directive 2010/63/EU for animal experiments. This study was approved by the Beihua University Medical Ethics Review Committee. Informed consent was obtained in writing from all the individual participants included in the study.

Consent for publication

Not applicable.

Competing interests

The author(s) declare no competing interests.

References

1. FRYDMAN A, SIMONIAN K. Review of models for titanium as a foreign body[J]. J Calif Dent Assoc, 2014, 42(12): 829–833.
2. Lai-Chang Zhang, Liu Y , Li S , et al. Additive Manufacturing of Titanium Alloys by Electron Beam Melting: A Review[J]. Advanced Engineering Materials, 2018, 20(5).
3. JIN He-xi, WEI Ke-xiang, LI Jian-ming, ZHOU Jian-yu, PENG Wen-jing. Research development of titanium alloy in aerospace industry[J]. The Chinese Journal of Nonferrous Metals, 2015, 25(2): 280–292.
4. Amer M A R , Pablo A Rodríguez, Renou S J , et al. Use of Human Fascia Lata in Rat Calvarial Bone Defects[J]. Acta Odontologica Latinoamericana Aol, 2015, 28(3):231.
5. Deng L, Zhao X , Wei C, et al. Application of a three-dimensional printed segmental scapula prosthesis in the treatment of scapula tumors[J]. Journal of International Medical Research, 2019, 47(11):5873-5882.
6. Bandyopadhyay A , Mitra I , Bose S. 3D Printing for Bone Regeneration[J]. Current Osteoporosis Reports, 2020, 18(5):1-10.
7. Pei, Xuan Zhang, Boqing Fan, Yujiang et al. Bionic mechanical design of titanium bone tissue implants and 3D printing manufacture [J]. Materials Letters, 2017, 208(dec.1):133-137.
8. Levine B . A New Era in Porous Metals: Applications in Orthopaedics[J]. Advanced Engineering Materials, 2010, 10(9):788-792

9. Ting Liu, Yu Chen, Antonio Apicella, et al.Effect of Porous Microstructures on the Biomechanical Characteristics of a Root Analogue Implant: An Animal Study and a Finite Element Analysis[J]. ACS Biomaterials Science And Engineering, 2020, 6(11):6356-6367
10. FROST H M.A 2003 update of bone physiology and Wolff's Law for clinicians [J].The Angle Orthodontist,2004, 74(1):3-15.
11. Li G , Wang L , Pan W , et al. In vitro and in vivo study of additive manufactured porous Ti6Al4V scaffolds for repairing bone defects[J]. Rep, 2016, 6:34072.
12. Melchels F P W , Domingos M A N , Klein T J . Additive manufacturing of tissues and organs[J]. Progress in Polymer Science, 2012.
13. Chlebus E , Kuznicka B , Kurzynowski T , et al. Microstructure and mechanical behaviour of Ti—6Al—7Nb alloy produced by selective laser melting[J]. Materials Characterization, 2011, 62(5):488-495.
14. Parthasarathy J , Starly B , Raman S , et al. Mechanical evaluation of porous titanium (Ti6Al4V) structures with electron beam melting (EBM)[J]. J Mech Behav Biomed Mater, 2010, 3(3):249-259.
15. Plyusnin A , Kulkova J , Arthurs G , et al. Biological response to an experimental implant for tibial tuberosity advancement in dogs: A pre-clinical study[J]. Research in Veterinary Science, 2019, 128.
16. Luangphakdy V , Walker E , Shinohara K , et al. Evaluation of Osteoconductive Scaffolds in the Canine Femoral Multi-Defect Model[J]. Tissue Engineering Part A, 2013, 19(5-6):634-648.
17. Rasmussen J , TRholm S , Zee M D . Computational analysis of the influence of seat pan inclination and friction on muscle activity and spinal joint forces[J]. International Journal of Industrial Ergonomics, 2009, 39(1):52-57.
18. Pierre-Luc Sylvestre,Isabelle Villemure,Carl-Éric Aubin. Finite element modeling of the growth plate in a detailed spine model[J]. Medical & Biological Engineering & Computing,2007,45(10).
19. Rho J Y , Kuhn-Spearing L , Zioupos P . Mechanical properties and the hierarchical structure of bone. [J]. Medical Engineering & Physics, 1998, 20(2):92.
20. General Administration of quality supervision, inspection and Quarantine of the people's Republic of China. Inertial parameters of adult human body. National standards of the people's Republic of China. GB/T 17245-2004. 2004.
21. Jabir R A, Fransiskus M A, Ifran S, et al. The Needs of Current Implant Technology in Orthopaedic Prosthesis Biomaterials Application to Reduce Prosthesis Failure Rate[J]. Journal of Nanomaterials, 2016, 2016:1-9.
22. Kendell M. Pawelec,* Shatadru Chakravarty, Jeremy M. L. Hix, et al. Design Considerations to Facilitate Clinical Radiological Evaluation of Implantable Biomedical Structures[J]. ACS Biomaterials Science And Engineering, 2021, 7(2):718-726.
23. Bandyopadhyay A, Mitra I, Bose S.3D Printing for Bone Regeneration[J]. Current Osteoporosis Reports, 2020, 18(5):1-10.

Figures

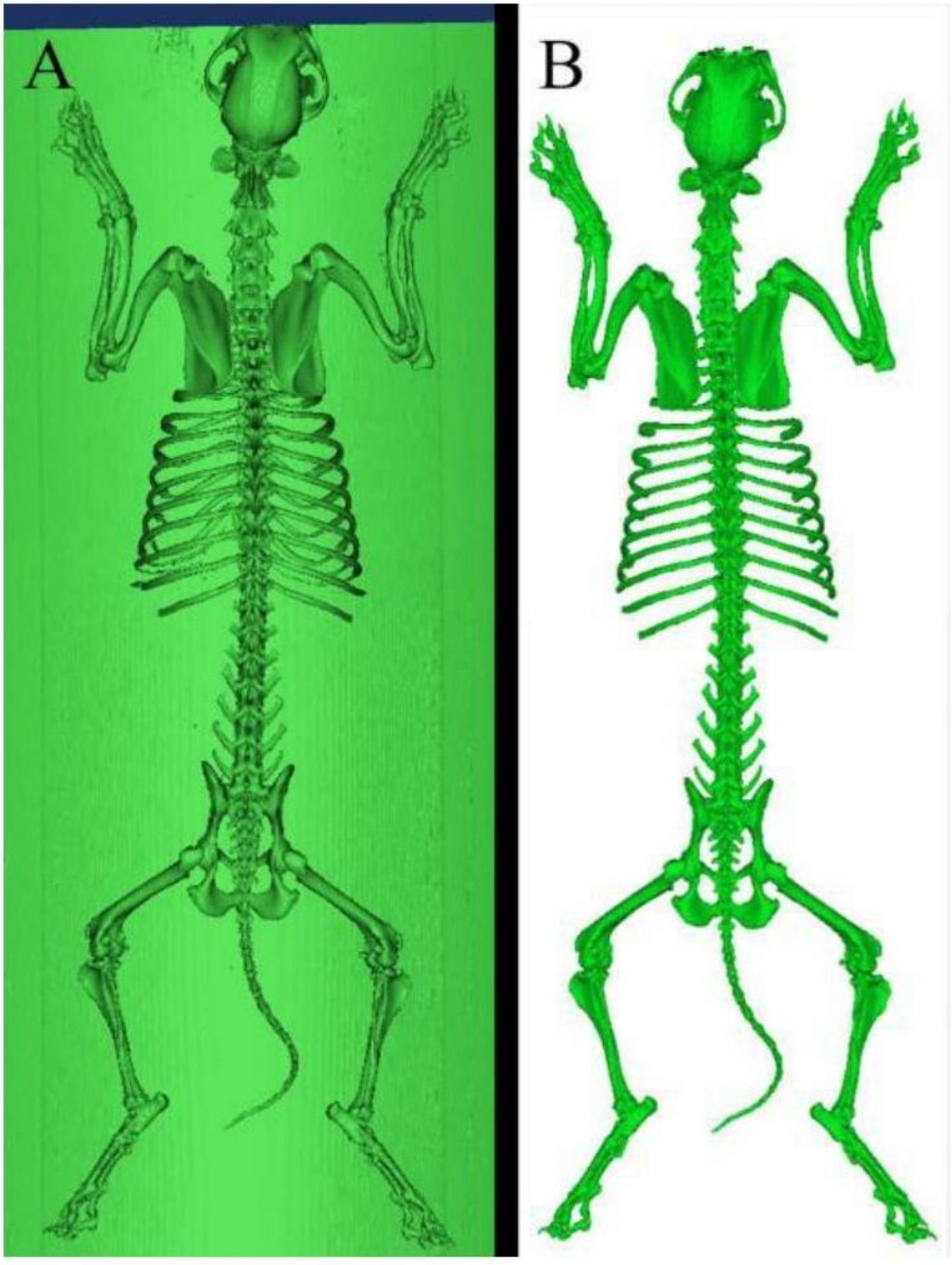

Figure 1

Processing of CT scan model of experimental dogs

A. CT model before processing B. CT model after processing

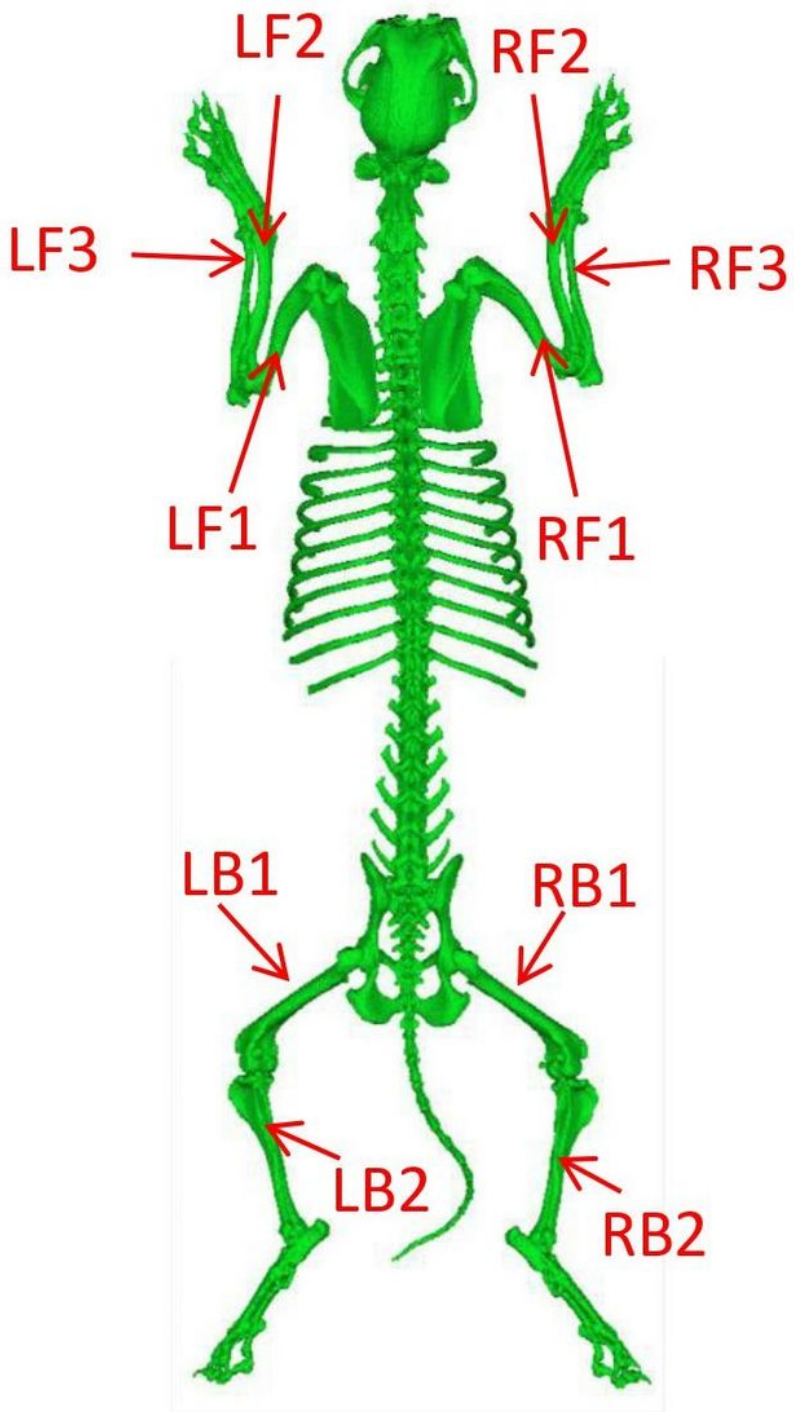

Figure 2

Number of main research bones

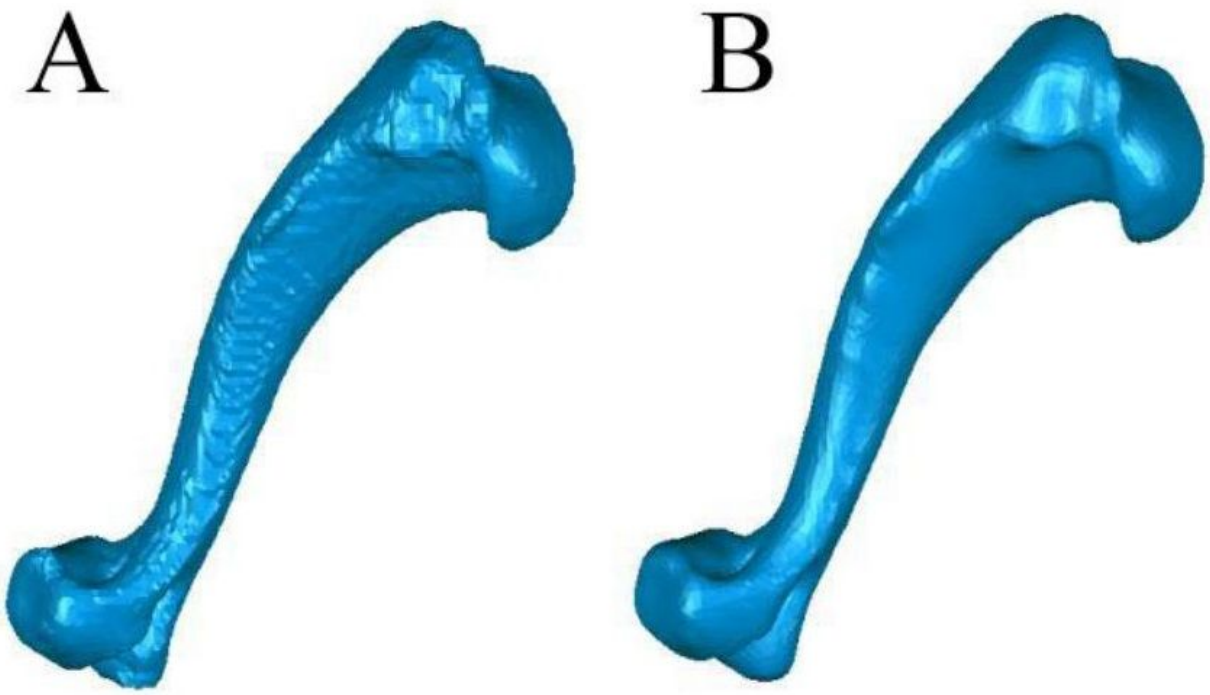

Figure 3

Processing of the CT scan model of main research bones（LF1）

A. Bone model before processing B. Bone model before processing

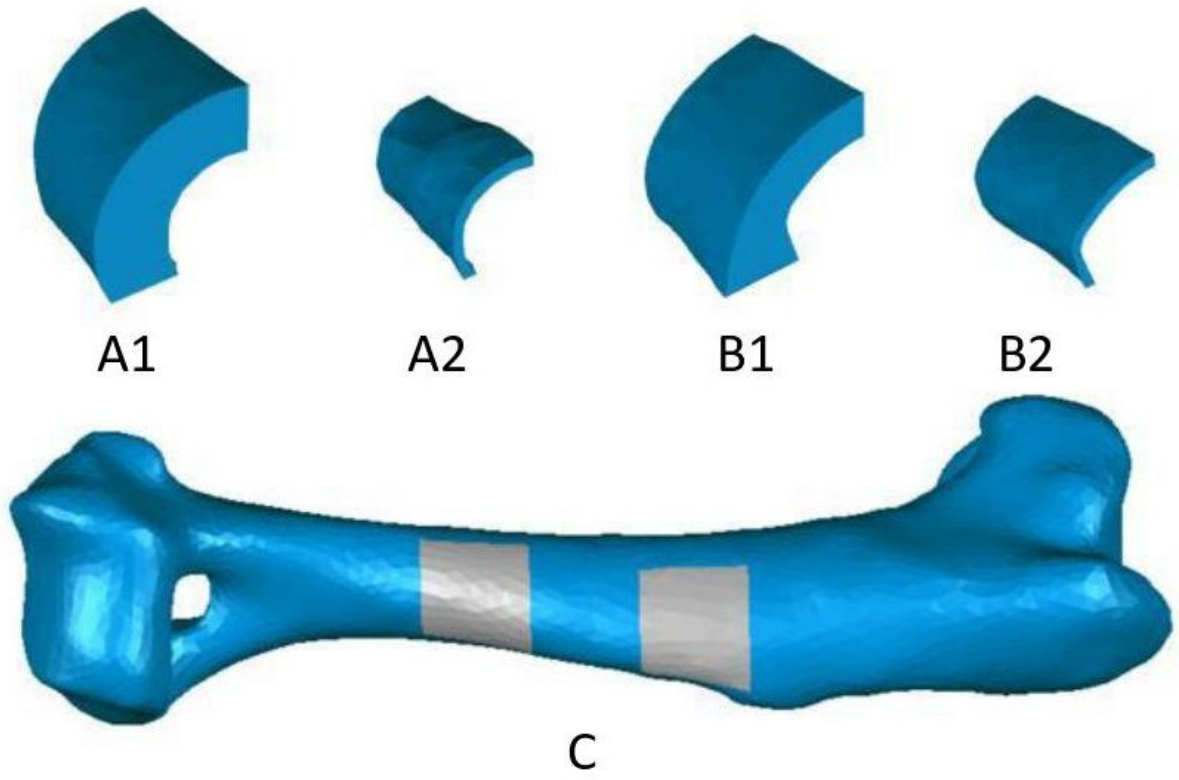

Figure 4

Implanted prosthesis models

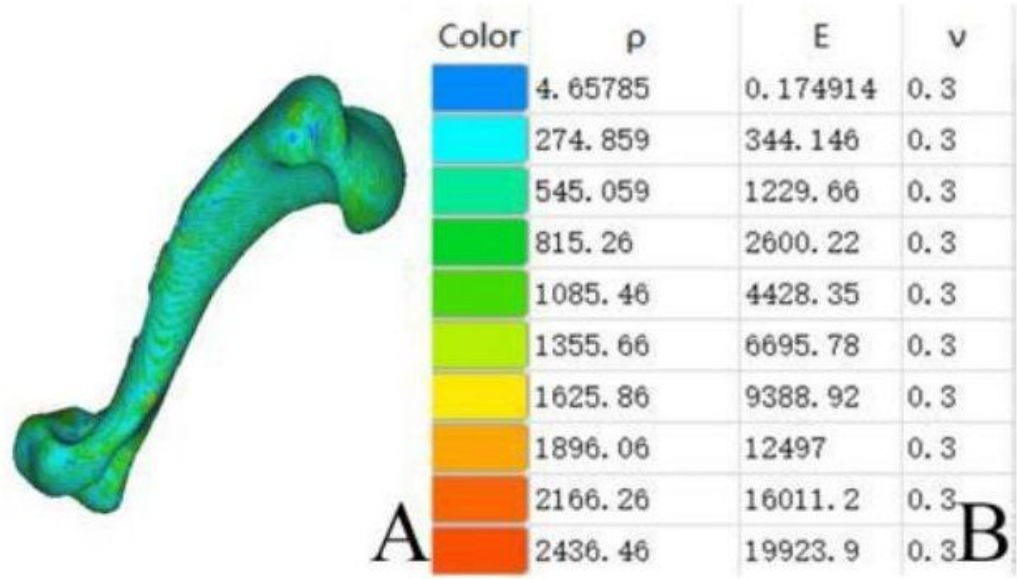

Color	ρ	E	ν
	4.65785	0.174914	0.3
	274.859	344.146	0.3
	545.059	1229.66	0.3
	815.26	2600.22	0.3
	1085.46	4428.35	0.3
	1355.66	6695.78	0.3
	1625.86	9388.92	0.3
	1896.06	12497	0.3
	2166.26	16011.2	0.3
	2436.46	19923.9	0.3

Figure 5

Assignment of material properties of the bones

A. Assignment effects B. Material properties

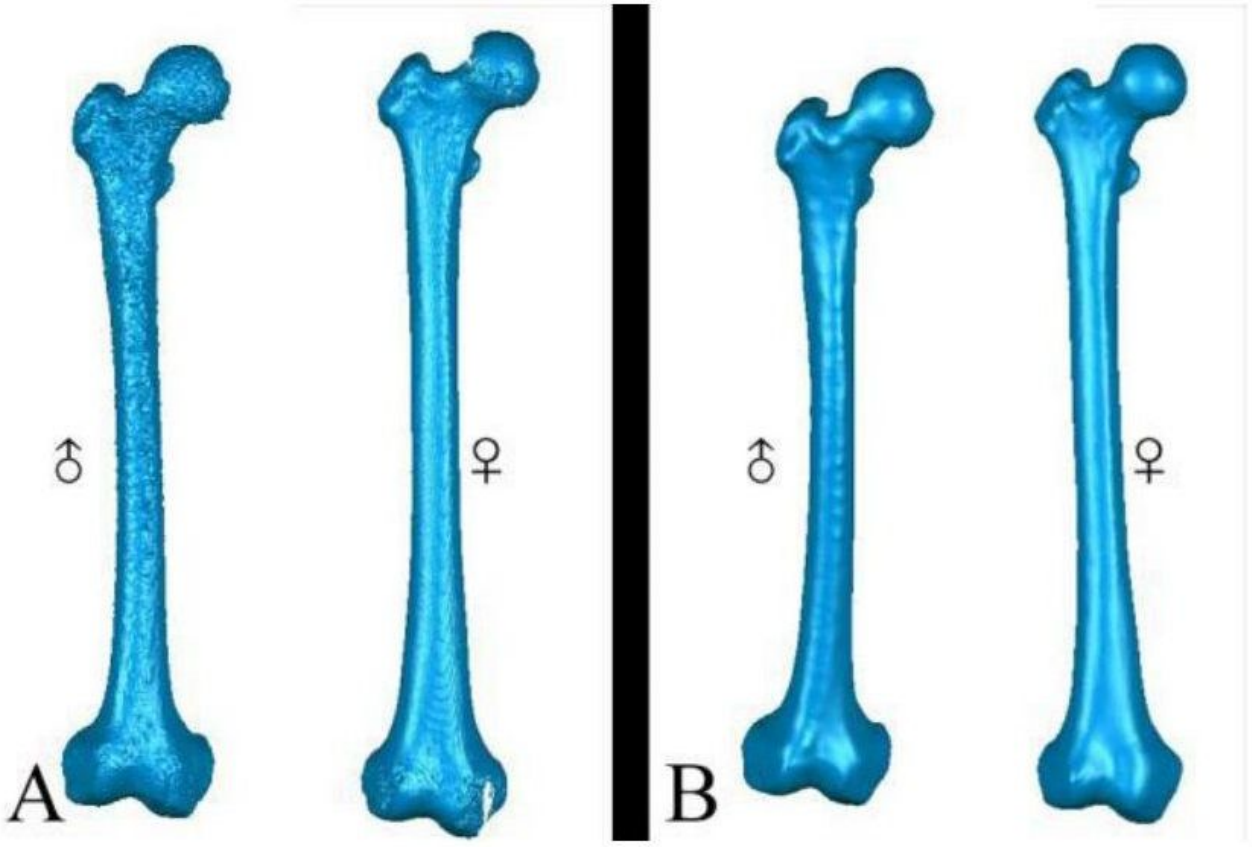

Figure 6

Processing of human bone models

A. Models before processing B. Models after processing

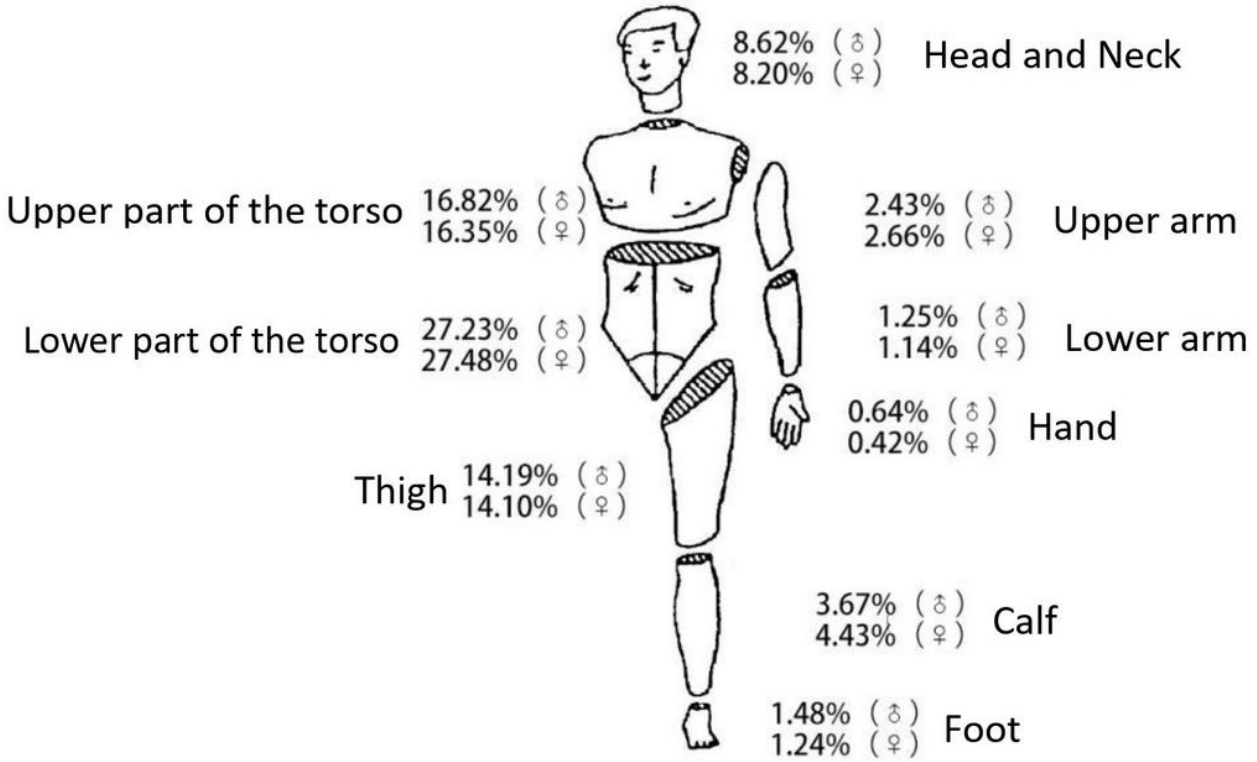

Figure 7

Mass distribution of Chinese people

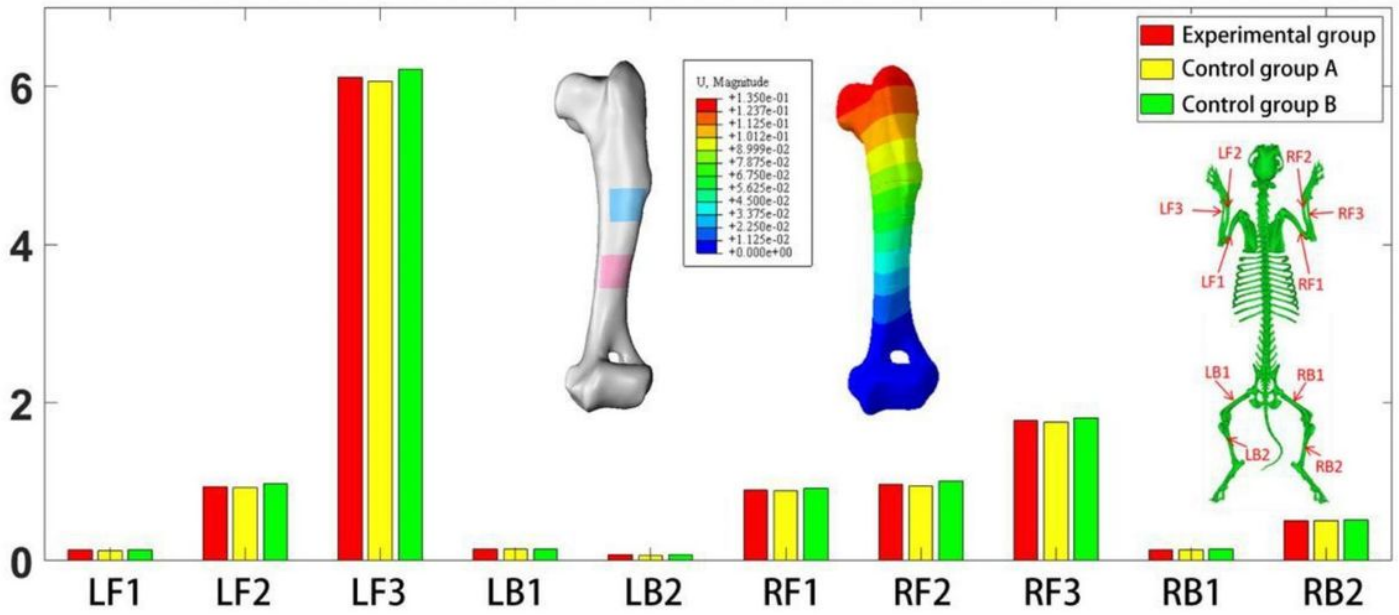

Figure 8

Displacement changes

LF1, LF2, LF3, LB1, LB2, RF1, RF2, RF3, RB1, RB2 are Number of main research bones

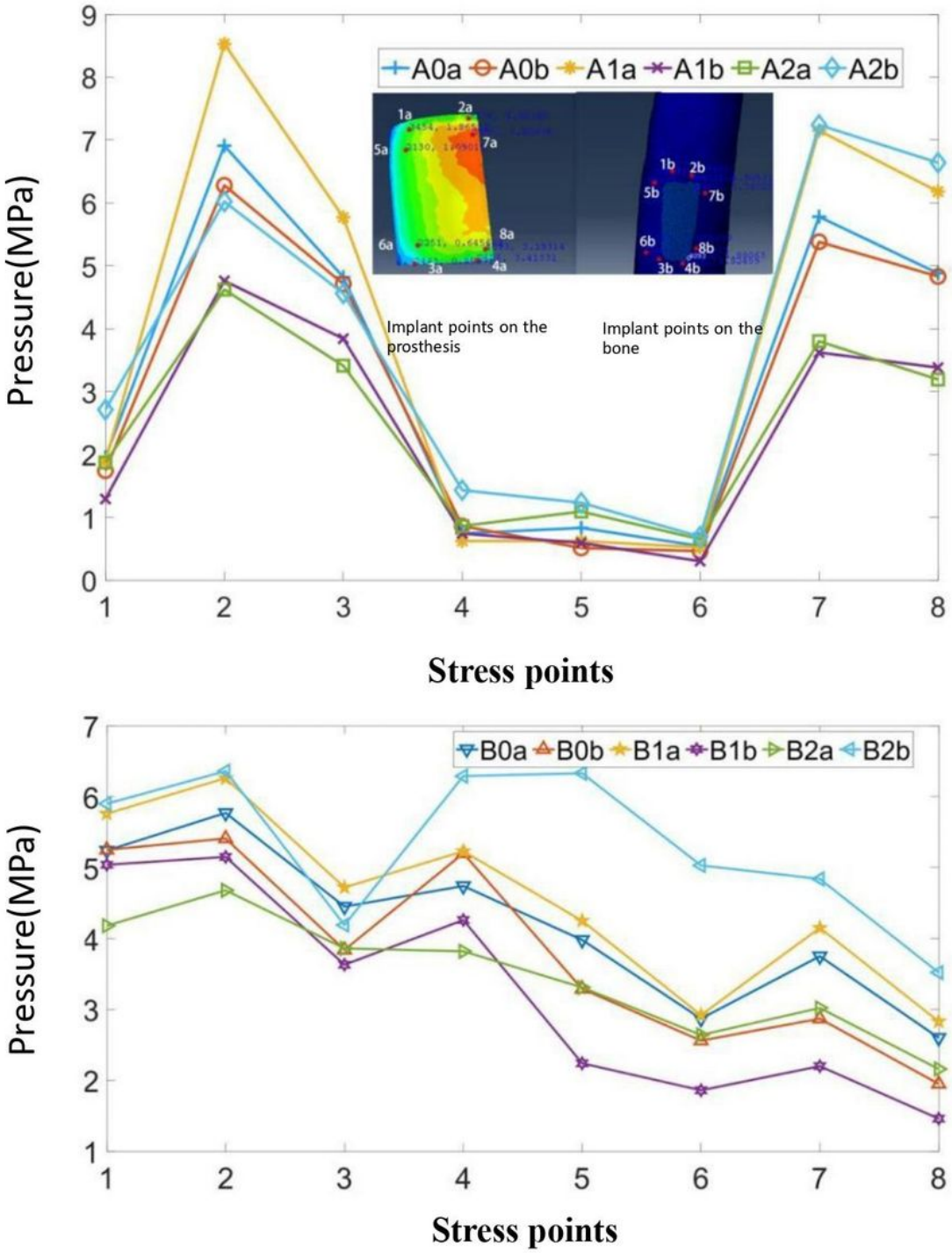

Figure 9

Selection of stress points and stress distribution

A. Stress distribution of male bone model, B. Stress distribution of female bone model